JOURNAL OF AIRCRAFT
Vol. 31, No. 4, July–Aug. 1994

Low-Speed Characteristics for the Wing-Canard Configuration of the International Vortex Flow Experiment

D. Hummel*
Institut für Strömungsmechanik, Braunschweig D-38106, Germany
and
H.-Chr. Oelker†
Dornier Luftfahrt GmbH, Wessling D-82230, Germany

Comprehensive aerodynamic investigations have been carried out on the coplanar wing-canard configuration of the International Vortex Flow Experiment (VFE) in symmetrical flow at low speed. Results of three-component balance, surface-pressure, and flowfield measurements are presented for the canard-off and the canard-on configuration. The vortex systems of canard and wing remain separate from each other. The main interference effects take place over the wing. The formation of the wing vortices is delayed to positions downstream of the apex. The canard vortices pass the wing leading edge relatively high, and after the onset of the wing vortices they are moved inward and downward over the wing. The trailing vortex sheet of the canard merges with the upper surface boundary layer in the inner portion of the wing. Considerably reduced vorticity is shed from the side-edges of the wing. This leads to a characteristic deformation of the vortex sheet in this region on the canard-off configuration, and to the formation of a side-edge vortex on the canard-on configuration. These results represent the limiting case $M \Rightarrow 0$ within the VFE.

Nomenclature

Geometric Quantities

$\bar{c}_W$ = mean aerodynamic chord of the wing
S = area of canard or wing extended to $y_C = y_W = 0$; Fig. 1
s = half-span of canard or wing
$s_1(x)$ = local half-span of canard or wing
t = maximum thickness of canard or wing or fuselage
t_E = local thickness at leading edge and trailing edge of canard and wing, t_{EC}, t_{EW}
x, y, z = body-fixed coordinates, origin at canard or wing or fuselage apex
x', z' = body-fixed coordinates, origin at the leading edge
$\bar{y}, \bar{z}$ = aerodynamic coordinates (normal to freestream) in the measuring plane, y, $z/\cos\alpha$
η = dimensionless local spanwise coordinate for canard or wing, y/s_1
$\bar{\eta}_C, \bar{\zeta}_C$ = dimensionless aerodynamic coordinates with the origin at the intersection of the measuring plane and the x_W axis, based on canard half-span; $\bar{y}_W/s_C$, $\bar{z}_W/s_C$
$\tilde{\eta}_W, \tilde{\zeta}_W$ = dimensionless aerodynamic coordinates with the origin at the intersection of the measuring plane and the x_W axis, based on local half-span of the wing; $\bar{y}_W/s_{1W}$, $\bar{z}_W/s_{1W}$
$\bar{\eta}_W, \bar{\zeta}_W$ = dimensionless aerodynamic coordinates with the origin at the intersection of the measuring plane with an axis parallel to the freestream that passes through the point $x_W = c_{iW}$, $y_W = 0$, $z_W = 0$ at the trailing edge of the wing; $\bar{y}_W/s_W$, $\bar{z}_W/s_W - (x_W - c_{iW})\sin\alpha/s_W$
ξ = dimensionless body-fixed coordinate for canard or wing

Aerodynamic quantities

c_D = drag coefficient, $D/q_\infty S_W$
c_L = lift coefficient, $L/q_\infty S_W$
c_m = pitching moment coefficient, reference point N_{25W}, nose-up positive, $M/q_\infty S_W \bar{c}_W$
c_p = static pressure coefficient, $(p - p_\infty)/q_\infty$
c_{pt} = total pressure coefficient, $(p_t - p_\infty)/q_\infty$
c_q = dynamic pressure coefficient, q/q_∞
p = static pressure
p_t = total pressure
q = dynamic pressure
$v_{\bar{y}}, v_{\bar{z}}, v_{\bar{y}\bar{z}}$ = velocity components in the $\bar{y}$-$\bar{z}$ plane, measuring plane
M = freestream Mach number
Re = freestream Reynolds number, based on c_{iW}
α = angle of attack, angle between freestream and wing plane, $z_W = 0$
$\Omega_{\bar{x}}$ = dimensionless axial vorticity, $\omega_{\bar{x}} s_W/V_\infty$
$\omega_{\bar{x}}$ = axial vorticity, normal to the $\bar{y}$-$\bar{z}$ plane, (measuring plane); $\frac{1}{2}(\partial v_{\bar{z}}/\partial\bar{y} - \partial v_{\bar{y}}/\partial\bar{z})$

Subscripts

C = canard
F = fuselage
W = wing
∞ = freestream conditions

I. Introduction

CLOSE-COUPLED canard-wing configurations play an important role in modern fighter aircraft design. The benefits of such a "tail arrangement" are known since the study by Behrbohm.[1] The maximum lift coefficient $c_{L\max}$ and the corresponding angle of attack $\alpha(c_{L\max})$ are considerably increased by adding a canard to a slender wing. This advantage is due to favorable interference effects between the vortex systems of canard and wing.[1] A large number of experimental investigations on series of canard-wing combinations is available in the literature that has been collected by Oelker.[2]

Received May 6, 1993; revision received Sept. 1, 1993; accepted for publication Sept. 2, 1993.

*Prof. Dr.-Ing., Technische Universität Braunschweig, Bienroder Weg 3.
†Dr.-Ing., Flight Test, Postfach 1103.

Investigations on the physics of the interfering vortex systems of canard and wing are rare. Some qualitative informations may be taken from Refs. 3–5. Quantitative work related to the flowfield was done by Griffin et al.,[6–8] and Hummel and Oelker.[9–12] According to these investigations the interference mechanism at low speed may be regarded as understood. The canard induces at the wing a nonuniform distribution of local angles of attack, which leads to a nonconical vortex formation at the wing and to a delay in the occurrence of wing vortex breakdown. On the other hand, the wing produces upwash at the canard, which increases its lift. Another favorable effect at the canard results from longitudinal velocity components induced by the wing that lead to a delay of canard vortex breakdown. Details may be taken from Ref. 11.

In 1984 the International Vortex Flow Experiment (VFE) was initiated by Drougge[13] in order to provide high-quality experimental results for code validation at both high and low speed. A canard-wing configuration has been studied that consisted of an $A_C = 1.65$ ($\varphi_{CL} = 60$ deg) canard in coplanar combination with an $A_W = 1.38$ ($\varphi_{WL} = 65$ deg) cropped delta wing and coupled by a small fuselage on the lower side. The geometry of this configuration has been described by Drougge[13] and Elsenaar et al.[14] Force and pressure distribution measurements as well as qualitative flow visualizations on the surface of the configuration and in the flowfield, carried out by the members of the international working group in the Mach number range $0.4 \leq M \leq 2.2$, are summarized in Ref. 14. The Institut für Strömungsmechanik of TU Braunschweig took part in the VFE.[13] An already existing wind-tunnel model[9] was equipped with the original $A_C = 1.65$ canard and the $A_W = 1.38$ sharp-edged cropped delta wing of the VFE configuration in a coplanar arrangement. The existing thin flat fuselage was used rather than the original body of the VFE configuration. Three-component balance and pressure distribution measurements, flow visualizations, as well as flowfield measurements have been carried out for this configuration at low speed, and within the VFE these measurements represent the limiting case $M \Rightarrow 0$. It is the purpose of this article to publish the main results of these investigations. A set of data will be provided that can be used as an experimental background for comparison with theoretical investigations.

The main aim of the VFE was the validation of computer codes from experiments. This has been done within the international working group for solutions of the Euler equations as indicated in Refs. 13 and 14. This work has been continued[15–18] and extended to solutions of the Navier-Stokes equations,[15,19,20] and it can be expected that the number of numerical investigations in this field will still increase. Therefore, the experimental data from the VFE and related investigations will be used extensively in the future.

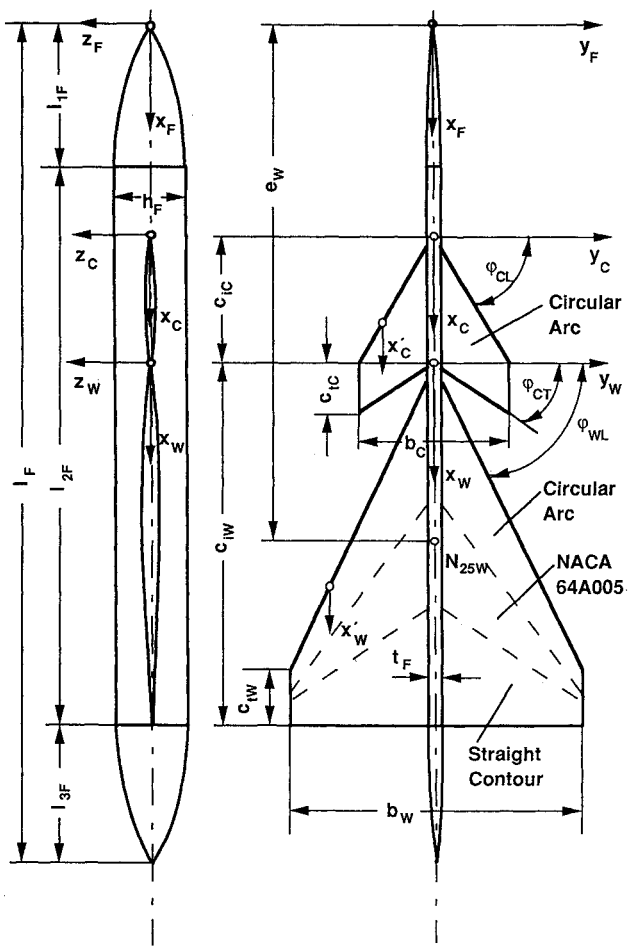

Fig. 1 Coplanar canard-wing-fuselage configuration.

II. Experimental Setup and Test Program

The measurements have been carried out in the 1.3-m low-speed wind tunnel of Institut für Strömungsmechanik at TU Braunschweig. This closed-circuit wind tunnel has an open test section of circular shape.

A. Wind-Tunnel Model

The investigations have been performed on a coplanar canard-wing-body configuration that is shown in Fig. 1. The geometric data may be taken from Table 1.

The wing planform is identical to that according to the VFE,[13,14] but the airfoil sections are slightly different due to manufacturing peculiarities at the leading and trailing edges. The wing thickness at these edges was chosen as a constant $t_E/c_{iW} = 0.00289$ ($t_E = 1.5$ mm). As in the VFE, the basic airfoil in sections $y_W = \text{const}$ is NACA 64 A 005. The front part $0 \leq (x'/c)_W \leq 0.4$ is replaced by a circular arc that meets the point of maximum thickness of the airfoil at $(x'/c)_W = 0.4$ with horizontal tangent, and which passes the leading edge $(x'/c)_W = 0$ at $z'_W = t_E/2$. The rear part of the basic airfoil is replaced by a straight line that starts at the trailing edge ($x'/$

Table 1 Geometric data of the configuration

Canard	
Aspect ratio	$A_C = b_C^2/S_C = 1.65$
Taper ratio	$\lambda_C = c_{tC}/c_{iC} = 0.40$
Leading-edge sweep	$\varphi_{CL} = 60$ deg
Trailing-edge sweep	$\varphi_{CT} = 35$ deg
Thickness ratio	$(t/c_i)_C = 0.05$
Wing	
Aspect ratio	$A_W = b_W^2/S_W = 1.38$
Taper ratio	$\lambda_W = c_{tW}/c_{iW} = 0.15$
Leading-edge sweep	$\varphi_{WL} = 65$ deg
Trailing-edge sweep	$\varphi_{WT} = 0$ deg
Geometric neutral point N_{25W}	$x_{N25W}/c_{iW} = 0.49$
Thickness ratio	$(t/c_i)_W = 0.05$
Fuselage	
Length/height ratio	$l_F/h_F = 12$
Length/thickness ratio	$l_F/t_F = 60$
Front and rear part length	$l_{1F}/h_F = l_{3F}/h_F = 2$
Central part length	$l_{2F}/h_F = 8$
Combination wing—fuselage	
Relative fuselage length	$l_F/b_W = 2.91$
Relative fuselage width	$t_F/b_W = 0.049$
Position of N_{25W}	$e_W/l_F = 0.612$
Combination canard—wing	
Relative canard size	$b_C/b_W = 0.44$
Position: coplanar; wing's leading edge meets canard's trailing edge at $y = 0$.	

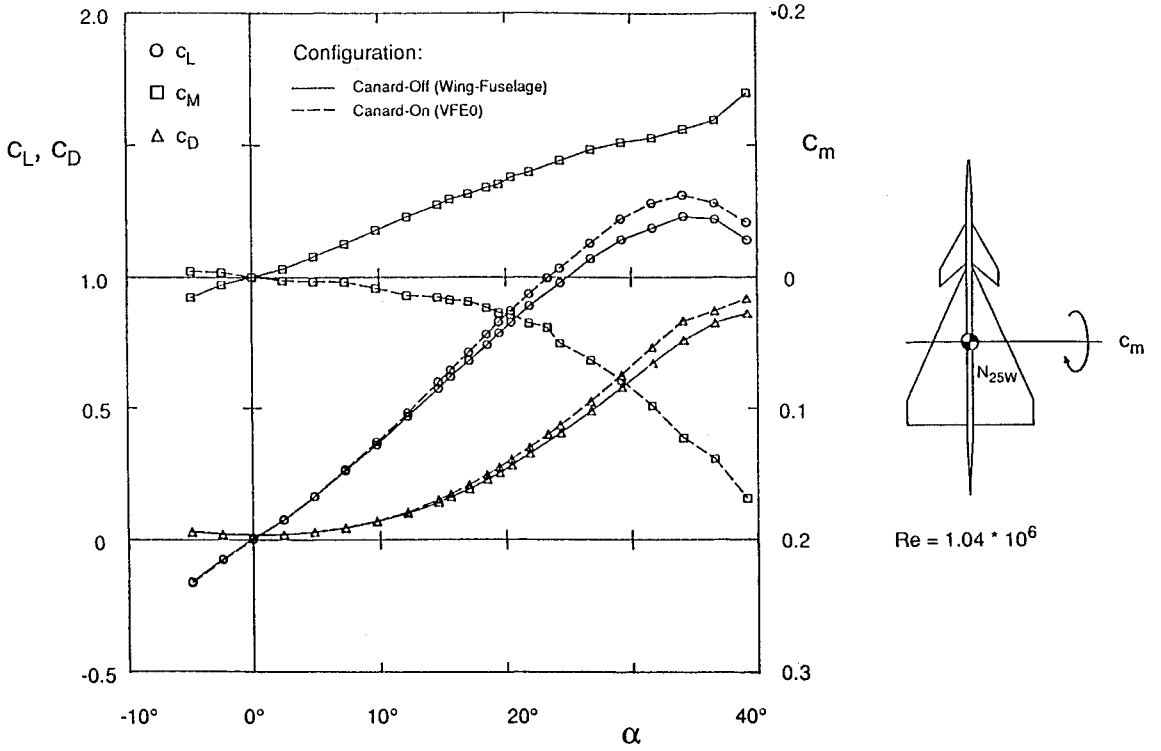

Fig. 2 Results of three-component balance measurements for the canard-off and the canard-on configuration at $Re = 1.04 \times 10^6$.

$c)_W = 1.0$ at $z'_W = t_E/2$, and which meets the basic airfoil contour continuously with respect to slope. The distribution of the three areas with circular arc, NACA 64 A 005 airfoil, and straight line contour on the wing is shown in Fig. 1. The deviations from the original VFE wing are small and the leading and trailing edges of the wing may be regarded as aerodynamically sharp. The wind-tunnel model was produced with $c_{iW} = 0.52$ m.

The canard planform is again identical to that of the VFE.[13,14] The airfoil sections are symmetric circular arc profiles with a thickness ratio $(t/c)_C = 0.05$. Their contour is chosen in such a way that the leading edge $(x'/c)_C = 0$ and the trailing edge $(x'/c)_C = 1.0$ are passed at $z'_C = t_E/2$ with $t_E/c_{iW} = 0.00289$ ($t_E = 1.5$ mm).

Both wing and canard are equipped with a tube system underneath the surface, and pressure holes in order to measure the surface pressure distribution. On the wing the pressure tabs are arranged on lines $\xi_W = \text{const}$ in the region $0.20 \leq \xi_W \leq 0.95$ in steps $\Delta\xi_W = 0.05$, and their spanwise distance was $\Delta\eta_W = 0.1$ for $0.20 \leq \xi_W \leq 0.45$, and $\Delta\eta_W = 0.05$ for $0.50 \leq \xi_W \leq 0.95$. On the canard the pressure tabs are located on lines $\xi_C = \text{const}$ in the region $0.5 \leq \xi_C \leq 1.0$ in steps $\Delta\xi_C = 0.1$, and their spanwise distance is $\Delta\eta_C = 0.1$.

In the wind-tunnel model a thin flat fuselage is used to keep the canard in position relative to the wing, and to cover some volume necessary for the rubber tubes in case of pressure distribution measurements. The fuselage consists of a cylindrical portion of length $l_{2F} = 8h_F$ with basically rectangular cross section $h_F = 5t_F$ that is modified by an edge radius $r_F = t_F/4$. Attached are front and rear parts of length $l_{1F} = l_{3F} = 2h_F$. Their shapes with respect to height and thickness have been chosen as polynomials of fourth-order that meet the cylindrical part continuously with respect to slope and curvature. The fuselage model was produced with $l_F = 1.20$ m.

The wing was added to the fuselage in such a way that the trailing edge coincided with the rear end of the cylindrical part of the fuselage. Concerning the canard-wing combination, in the symmetry plane $y_C = y_W = 0$ the trailing edge of the canard was located at the leading edge of the wing. Canard and wing were arranged coplanar in the middle of the fuselage height. The dimensionless geometric data of the configuration may be taken from Table 1.

B. Description of the Tests

The wind-tunnel investigations have been carried out at freestream velocities of $V_\infty = 30$ and 40 m/s, which correspond to $Re = 1.04 \times 10^6$ and 1.40×10^6, and to $M = 0.086$ and 0.115.

For three-component balance measurements the wind-tunnel model was fixed in the test section by means of the customary wire suspension. In the course of the evaluation of the force measurements the usual corrections of the angle of attack have been taken into account. The angle-of-attack range $-5 \leq \alpha \leq 40$ deg has been covered at steps $\Delta\alpha = 2.5$ deg. The Reynolds number was 1.04×10^6.

For the pressure distribution and the flowfield measurements the model was fixed in the test section by means of thin cylindrical rods from the bottom side of the wing. In the pressure distribution measurements the rubber tubes left the model at the end of the fuselage and were guided from there downstream and then across the working section of the wind tunnel to the scanivalve pressure transducer system. The pressure distribution measurements have been carried out in such a way that the top side of the configuration was used as upper and lower surface, respectively. Results for $\alpha = 9.8$ deg are presented subsequently for which flowfield measurements have also been performed. The Reynolds number was 1.40×10^6.

Flowfield measurements have been carried out in planes perpendicular to the freestream using a conical five-hole probe of 2 mm diam, the probe hole diameter being 0.3 mm. These measurements were performed for $\alpha = 9.8$ deg, at which no vortex breakdown was present, at stations $\xi_W = 0.15$, 0.3, 0.6, 0.8, 1.01, and 1.125. The Reynolds number was 1.40×10^6.

In order to detect interference effects, three-component balance, pressure distribution, and flowfield measurements have also been carried out on the canard-off configuration. For direct comparison, pressure distribution and flowfield measurements have been performed for $\alpha = 9.8$ deg at $\xi_W = 0.8$, 1.01, and 1.125. In addition, the canard-off configuration has been investigated at $\alpha = 14.6$ deg, for which again, no vortex breakdown was present. Pressure distributions and flowfield measurements are presented for planes at $\xi_W = 0.8$, 1.01, and 1.125.

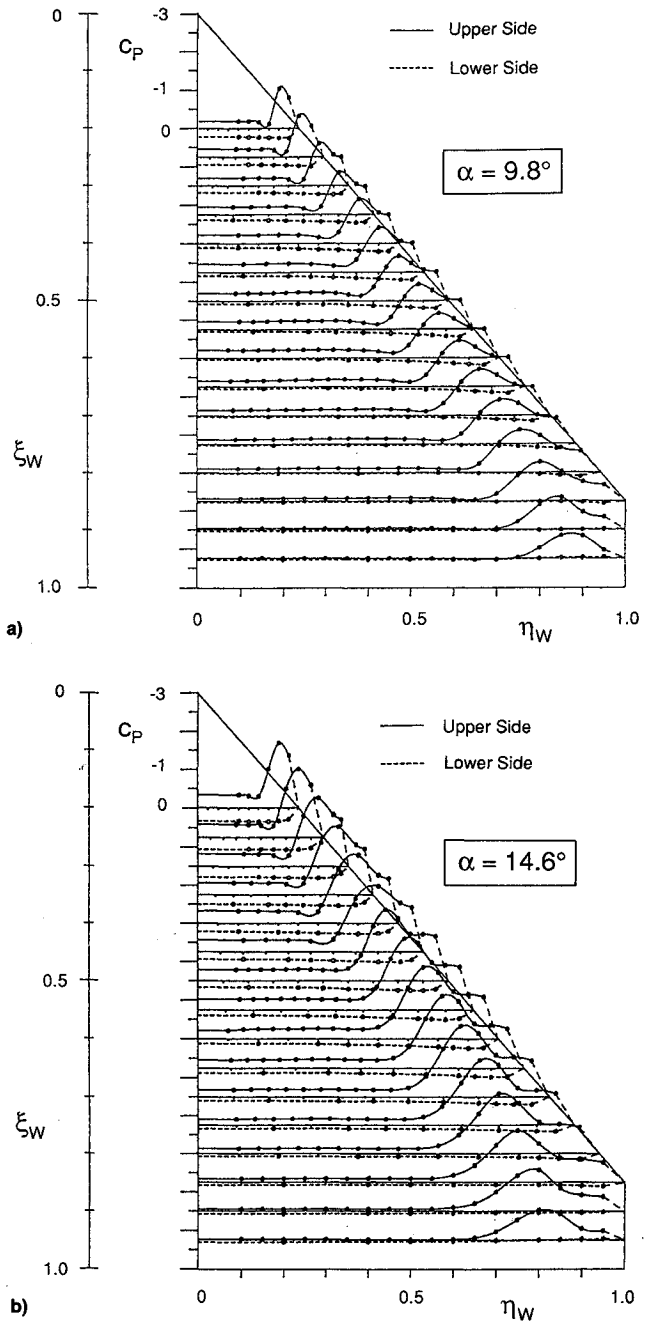

Fig. 3 Surface-pressure distribution on the canard-off configuration at $Re = 1.40 \times 10^6$ for a) $\alpha = 9.8$ and b) 14.6 deg.

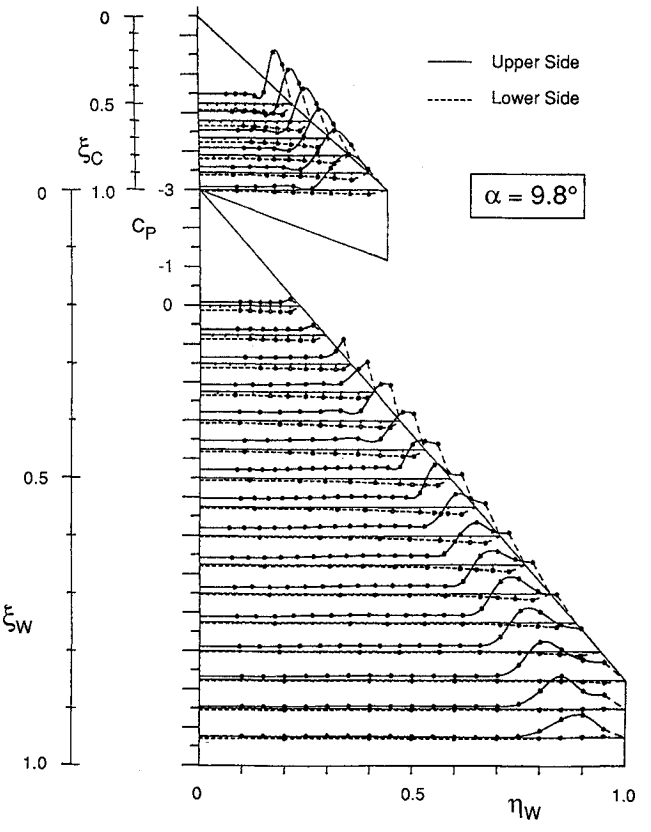

Fig. 4 Surface-pressure distribution on the canard-on configuration at $Re = 1.40 \times 10^6$ for $\alpha = 9.8$ deg.

III. Results

A. Force and Moment Coefficients

Results of the three-component balance measurements for the canard-off and the canard-on configuration are shown in Fig. 2. For low angles of attack both configurations have nearly the same lift and drag, but the addition of the canard to the wing-fuselage configuration changes the formerly nose-down pitching moment into a nose-up pitching moment. For large angles of attack the canard-on configuration reaches higher maximum lift coefficients than the canard-off configuration. This overall behavior of a canard configuration is well-known.[2,9]

B. Pressure Distributions

Following the status of the flow will be analyzed for cases in which no vortex breakdown is present over the configuration, neither within the canard vortices nor within the wing vortices. Measured pressure distributions are shown in Fig. 3 for the canard-off configuration at $\alpha = 9.8$ deg and 14.6 deg, and for the canard-on configuration at $\alpha = 9.8$ deg in Fig. 4. Some values of the measured pressure coefficients are given in Tables 2 and 3. The traces of the leading-edge vortices can be detected from the suction peaks on both configurations. Vortex breakdown does not take place at these angles of attack. The pressure distribution on the canard indicates that its vortices originate from the junction of the leading edge and the fuselage contour in the same way as on the wing of the canard-off configuration. The pressure distribution on the wing of the canard-on configuration, however, shows considerably lower suction in the front part, and the suction peaks lie closer to the leading edge than for the canard-off configuration. This can be seen more easily in Fig. 5 in a direct comparison of pressure distributions on the wing for the canard-on and -off configurations. This comparison is taken at the same measuring stations where the flowfield measurements presented in this article have been performed. For the canard-off configuration in all three sections a suction peak is present that results from a well-developed vortex. For the canard-on configuration, however, the small suction peak at $\xi_W = 0.3$ at the leading edge can be interpreted to be due to either an attached flow around the leading edge or a small vortex very close to the leading edge. At $\xi_W = 0.6$ the suction peak indicates a developed vortex for the canard configuration, and at $\xi_W = 0.8$ magnitude and position of the suction peak are about the same as for the canard-off configuration.

These results indicate that at this moderate angle of attack the effect of the wing on the canard is small and the canard acts like a small wing in free flow. On the other hand the canard induces behind its trailing edge a downwash field within its span and an upwash field outside its span. The downwash field reduces the effective angle of attack in the forward and inner portion of the wing considerably, and this leads to a suppression of flow separation there. The upwash field increases the effective angle of attack in the outer and rear portion of the wing, and this supports flow separation there. This mechanism leads to a delayed formation of the wing

Table 2 Values for c_p for the canard-off configuration at α = 9.8 and 14.6 deg

ξ_W	0.3		0.6		0.8	
η_W	Lower	Upper	Lower	Upper	Lower	Upper
			a) α = 9.8 deg			
0.10				−0.214		−0.101
0.15				−0.205		−0.103
0.20			0.041	−0.206	0.021	−0.105
0.25				−0.208		−0.111
0.30		−0.201		−0.211		−0.109
0.35				−0.215		−0.110
0.40	0.173	−0.202	0.047	−0.215	0.028	−0.108
0.45				−0.214		−0.108
0.50	0.183	−0.199	0.059	−0.213	0.024	−0.113
0.55				−0.200		−0.108
0.60	0.195	−0.162	0.068	−0.169	0.019	−0.087
0.65				−0.129		−0.074
0.70	0.206	−0.165	0.088	−0.328	0.023	−0.228
0.75				−0.862		−0.787
0.80	0.221	−1.104	0.123	−1.170	0.035	−1.117
0.85			0.144	−1.020	0.050	−0.963
0.90	0.230	−0.810	0.168	−0.807	0.082	−0.638
0.95			0.193	−0.758	0.118	−0.556
			b) α = 14.6 deg			
0.10				−0.171		−0.132
0.15				−0.243		−0.137
0.20			0.119	−0.255	0.068	−0.138
0.25				−0.258		−0.143
0.30		−0.319		−0.253		−0.139
0.35				−0.263		−0.137
0.40	0.279	−0.312	0.133	−0.267	0.077	−0.132
0.45				−0.263		−0.129
0.50	0.290	−0.283	0.149	−0.254	0.076	−0.130
0.55				−0.248		−0.138
0.60	0.299	−0.274	0.160	−0.305	0.077	−0.207
0.65				−0.610		−0.485
0.70	0.306	−1.299	0.183	−1.326	0.089	−1.063
0.75				−1.851		−1.590
0.80	0.303	−1.757	0.211	−1.716	0.102	−1.330
0.85			0.227	−1.218	0.117	−0.826
0.90	0.275	−1.331	0.241	−1.151	0.144	−0.770
0.95	0.182	−1.209	0.230	−1.089	0.157	−0.688

vortices on the canard configuration. Because of the nonuniform distribution of the effective angle of attack along the leading edge of the wing, the wing vortex is fed with vorticity in a different manner than is known from canard-off configurations. In total, the wing of a canard-on configuration works at a lower effective angle of attack, and this leads to a compensation of the additional lift at the canard through a loss of lift at the wing. Therefore, both configurations have almost the same lift as indicated in Fig. 2.

C. Documentation of the Three-Dimensional Flowfield for the Canard-Off Configuration

The documentation of the three-dimensional flowfield was carried out in several planes normal to the freestream and located at different longitudinal positions ξ_W. Due to the "conicality" of the flowfield, the results for ξ_W = 0.8 may be regarded as representative for the whole front part of the wing. Since a wing with a taper ratio $\lambda \neq 0$ is considered, some changes in the flow pattern may be expected in the rear part of the wing, and therefore, the positions ξ_W = 1.01 and 1.125, just behind the wing, were chosen.

An angle of attack of α = 9.8 deg has been considered in order to provide the possibility of a direct comparison with the canard-on configuration. Results for this angle of attack are shown in Fig. 6 by total pressure isobars, and in Fig. 7 by lines of constant axial vorticity in the three measuring planes. Another angle of attack, α = 14.6 deg, has been chosen in order to provide a set of data for a more developed vortical flowfield without vortex breakdown, which is well-suited for comparison with numerical investigations. Figures 8 and 9 show the corresponding results for total pressure and axial vorticity distributions, and in Fig. 10 for α = 14.6 deg the velocity distribution is given for one measuring plane at ξ_W = 1.01 by means of dynamic pressure isobars and the velocity vector component in the measuring plane.

The total pressure distributions in Figs. 6 and 8 indicate the total pressure losses in the center of the primary vortex as well as in the wake downstream of the trailing edge. The vorticity sheet emanating from all edges of the wing is documented by a relative minimum of total pressure that is marked in the figures by a dash-dotted line. Downstream of the wing the trailing vortex sheet rolls up into a counter-rotating trailing-edge vortex. This phenomenon is well-known and has been studied for delta wings by Hummel.[21] In the measuring plane at ξ_W = 0.8 the vortex formation is very similar to that on a delta wing as described in Ref. 11. The primary vortex is located at $\bar{\eta}_W$ = 0.81, $\bar{\zeta}_W$ = 0.10 and a secondary vortex at α = 9.8 deg is located at $\bar{\eta}_W$ = 0.93, $\bar{\zeta}_W$ = 0.05. This secondary vortex is rather small since the boundary layer on the wing beneath the primary vortex is turbulent. More downstream in the region $0.8 < \xi_W < 1$, however, there exists a characteristic difference to delta wings. The vortex sheet emanating from the side edge of the wing moves outboard, reaches a remarkable distance from the wing plane, and then turns suddenly around towards the primary vortex center. This shape is clearly indicated in Figs. 6 and 8 by the total pressure contours, and in Fig. 10a by the corresponding dynamic pressure contours in the plane ξ_W = 1.01 at the trailing edge.

Figures 7 and 9 show the distributions of axial vorticity in the measuring planes. Positive values denote the sense of

Table 3 Values for c_p for the canard-on configuration at α = 9.8 deg

ξ_C	0.5		0.8		1.0	
η_C	Lower	Upper	Lower	Upper	Lower	Upper
0.2				−0.121	0.035	−0.075
0.3		−0.242		−0.190		−0.086
0.4	0.160	−0.248	0.082	−0.193	0.054	−0.107
0.5	0.178	−0.243	0.093	−0.185	0.065	−0.102
0.6	0.188	−0.198	0.108	−0.133	0.076	−0.041
0.7	0.212	−0.301	0.131	−0.508	0.088	−0.574
0.8	0.240	−1.328	0.164	−1.217	0.105	−0.939
0.9	0.279	−1.017	0.208	−0.833	0.115	−0.540
ξ_W	0.3		0.6		0.8	
η_W	Lower	Upper	Lower	Upper	Lower	Upper
0.10				−0.202		−0.114
0.15				−0.210		−0.124
0.20			0.027	−0.216	0.015	−0.130
0.25				−0.222		−0.139
0.30		−0.166		−0.227		−0.143
0.35				−0.239		−0.148
0.40	0.107	−0.168	0.034	−0.250	0.021	−0.150
0.45				−0.258		−0.149
0.50	0.115	−0.174	0.047	−0.264	0.019	−0.152
0.55				−0.267		−0.154
0.60	0.122	−0.177	0.057	−0.270	0.016	−0.151
0.65				−0.268		−0.147
0.70	0.132	−0.180	0.080	−0.258	0.019	−0.147
0.75				−0.255		−0.377
0.80	0.139	−1.187	0.113	−0.570	0.034	−1.064
0.85			0.136	−1.088	0.051	−1.031
0.90	0.141	−0.335	0.159	−0.983	0.077	−0.698
0.95	0.135		0.181	−0.843	0.113	−0.605

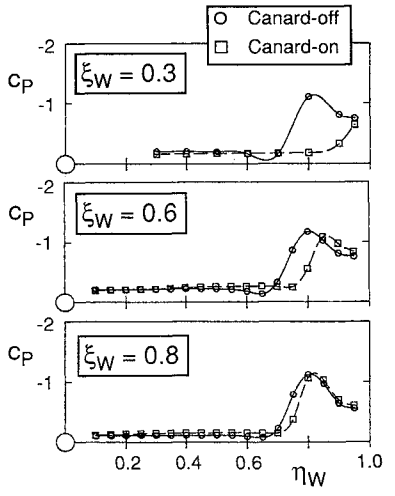

Fig. 5 Upper surface pressure distribution on the wing at α = 9.8 deg and Re = 1.40 × 10⁶. Direct comparison between the canard-off and the canard-on configuration at ξ_W = 0.3, 0.6, and 0.8.

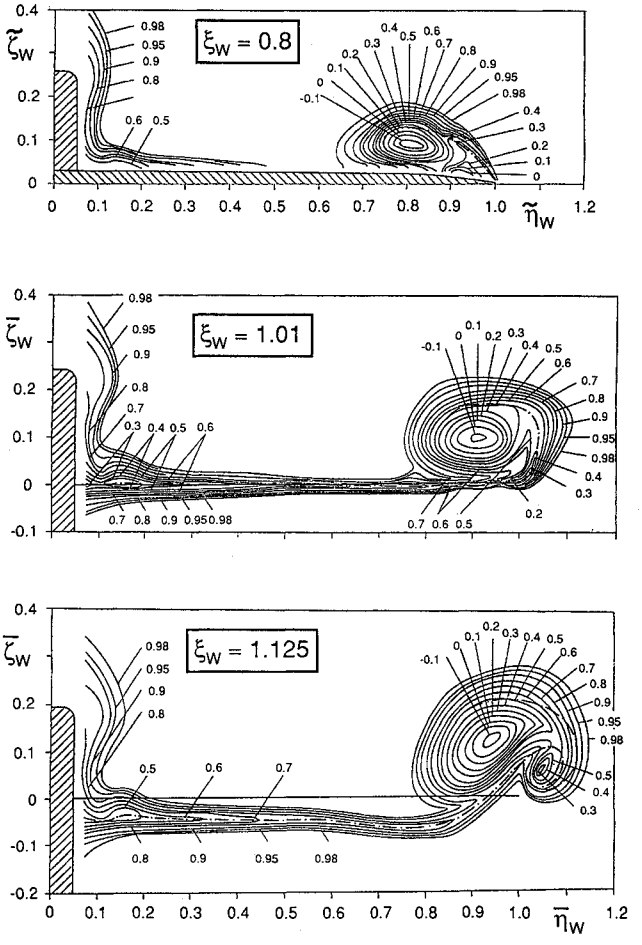

Fig. 6 Results of flowfield measurements over the canard-off configuration at α = 9.8 deg and Re = 1.40 × 10⁶. Total pressure isobars $c_{pt} = (p_t - p_\infty)/q_\infty$ = const at ξ_W = 0.8, 1.01, and 1.125.

rotation of the primary vortex according to Fig. 10b. In the plane at ξ_W = 0.8, the counter-rotating secondary vortex is marked by negative values of the axial vorticity. In the vortex sheet downstream of the wing's trailing edge, again, negative axial vorticity is present with a maximum in the region beneath the primary vortex. The formation of the counter-rotating trailing-edge vortex downstream of the wing is clearly indicated by the axial vorticity contours at ξ_W = 1.125. Concerning the distribution of axial vorticity in the vortex sheet emanating from the leading edge and from the side edge of the wing, the following results can be deduced. Upstream of the kink between leading edge and side edge in the plane at ξ_W = 0.8, the sense of rotation in the vortex sheet is the same as in the primary vortex. In the plane at the trailing edge, ξ_W = 1.01, the situation is different. In those parts of the vortex sheet far away from the wing, which originate from the leading

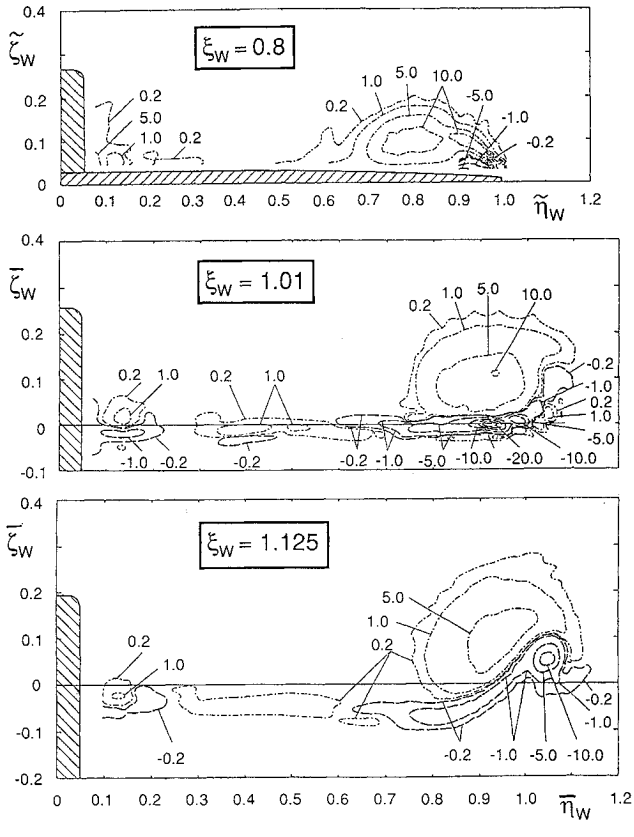

Fig. 7 Results of flowfield measurements over the canard-off configuration at α = 9.8 deg and Re = 1.40 × 10⁶. Lines of constant axial vorticity $\Omega_{\tilde{x}} = \omega_{\tilde{x}} \times s_W/V_\infty$ = const at ξ_W = 0.8, 1.01, and 1.125.

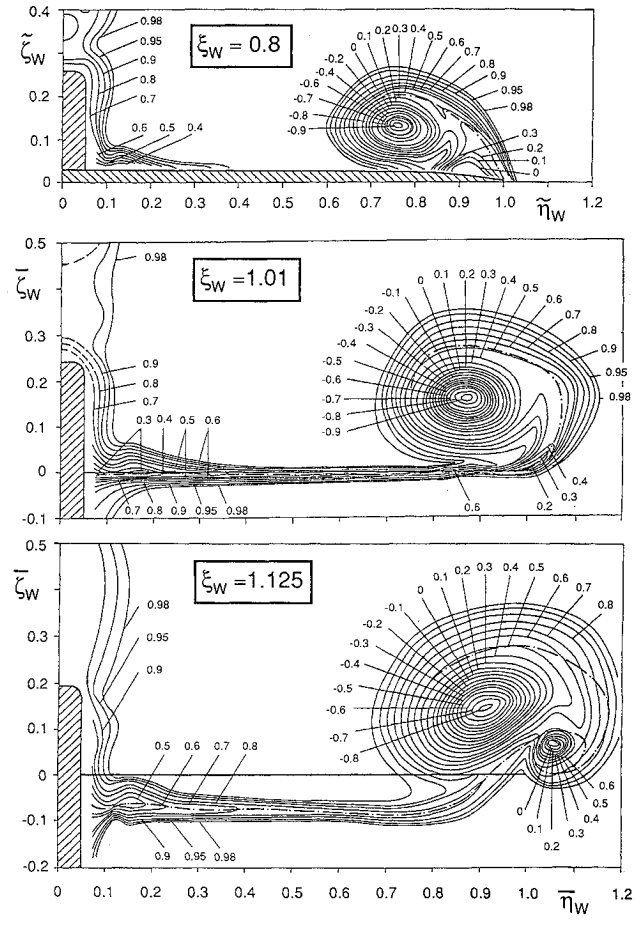

Fig. 8 Results of flowfield measurements over the canard-off configuration at α = 14.6 deg and Re = 1.40 × 10⁶. Total pressure isobars $c_{pt} = (p_t - p_\infty)/q_\infty$ = const at ξ_W = 0.8, 1.01, and 1.125.

edge, the sense of rotation is again the same as in the primary vortex. In those parts of the vortex sheet that start from the end of the leading edge and the beginning of the side edge, the shed vorticity is considerably reduced, and in the region close to the trailing edge the sense of rotation is even opposite. This does not necessarily mean that counter-rotating vorticity is shed from the side edge, since the secondary vortex passes over the side edge and might produce the negative axial vorticity there. The shape of the vortex sheet is mainly due to the mutual inductions between the different parts of the vortex sheet. It is the sudden drop of shed vorticity in the vortex sheet starting from the beginning of the side edge that leads to the outward and upward displacement of the vortex sheet that has been found in Figs. 6 and 8.

D. Documentation of the Three-Dimensional Flowfield for the Canard-On Configuration

The documentation of the three-dimensional flowfield for the canard-on configuration at α = 9.8 deg is given in Fig. 11 by total pressure contours, and in Fig. 12 by lines of constant axial vorticity in several planes normal to the freestream.

The first measuring plane at ξ_W = 0.15 is located just behind the trailing edge of the tip section of the canard. The canard vortex system is clearly indicated. It consists of the canard's primary vortex at $\tilde{\eta}_C$ = 0.94, $\tilde{\zeta}_C$ = 0.19 and the canard's trailing-edge vortex at $\tilde{\eta}_C$ = 1.05, $\tilde{\zeta}_C$ = 0.09, whereas the canard's secondary vortex cannot be detected. It is well-known from delta wings[21] that the secondary vortex is rather weak and that it merges into the trailing-edge vortex downstream of the trailing edge. At this small angle of attack there exists almost no influence of the wing on the canard. Therefore, the result in the plane at ξ_W = 0.15 may be regarded also as the documentation of the flow status behind the canard without interference. In the inner portion of the configuration the trailing vortex sheet of the canard joins the upper surface boundary layer of the wing. No separation takes place at the leading edge of the wing.

In the measuring plane at ξ_W = 0.3, the canard's trailing vortex sheet touches the upper surface of the wing for $\tilde{\eta}_W < 0.8$, and in this region the canard's vortex sheet and the wing's upper surface boundary layer are mixed. For $\tilde{\eta}_W > 0.8$, the vortex sheet is again separated from the wing and rolls into the canard's vortex system. The center of the canard's primary vortex is found at $\tilde{\eta}_W$ = 1.1, $\tilde{\zeta}_W$ = 0.4 by an absolute minimum of total pressure and an absolute maximum of positive (left rotating) axial vorticity. The trailing-edge vortex has turned around the primary vortex in the sense of rotation of the primary vortex and is now located at $\tilde{\eta}_W$ = 1.25, $\tilde{\zeta}_W$ = 0.53. During this process the corresponding total pressure losses and the axial vorticity are spread out and their intensities are considerably weakened. Due to the canard-induced downwash in this plane, no primary wing vortex could be detected here.

The results for the measuring plane at ξ_W = 0.6 show the mixed layer on the upper surface of the wing in the region $\tilde{\eta}_W < 0.55$. The canard's primary vortex is located at $\tilde{\eta}_W$ = 0.53, $\tilde{\zeta}_W$ = 0.32 and the remains of the counter-rotating trailing-edge vortex of the canard can be identified in Figs. 11 and 12 at $\tilde{\eta}_W$ = 0.48, $\tilde{\zeta}_W$ = 0.48. The canard's vortex system is now situated completely within the local span of the wing. Therefore, its induced velocities at the leading edge of the wing are directed upwards, and this situation favors flow separation there. At ξ_W = 0.6 a primary vortex is formed over the wing with its center at $\tilde{\eta}_W$ = 0.84, $\tilde{\zeta}_W$ = 0.08 and a corresponding secondary vortex can be identified from Fig. 12 by means of axial vorticities of opposite sign in a region very close to the surface at about $\tilde{\eta}_W$ = 0.9. The small secondary vortex indicates again that the boundary layer beneath the primary vortex is turbulent. A comparison with the results for the canard-off configuration up to the plane ξ_W = 0.6

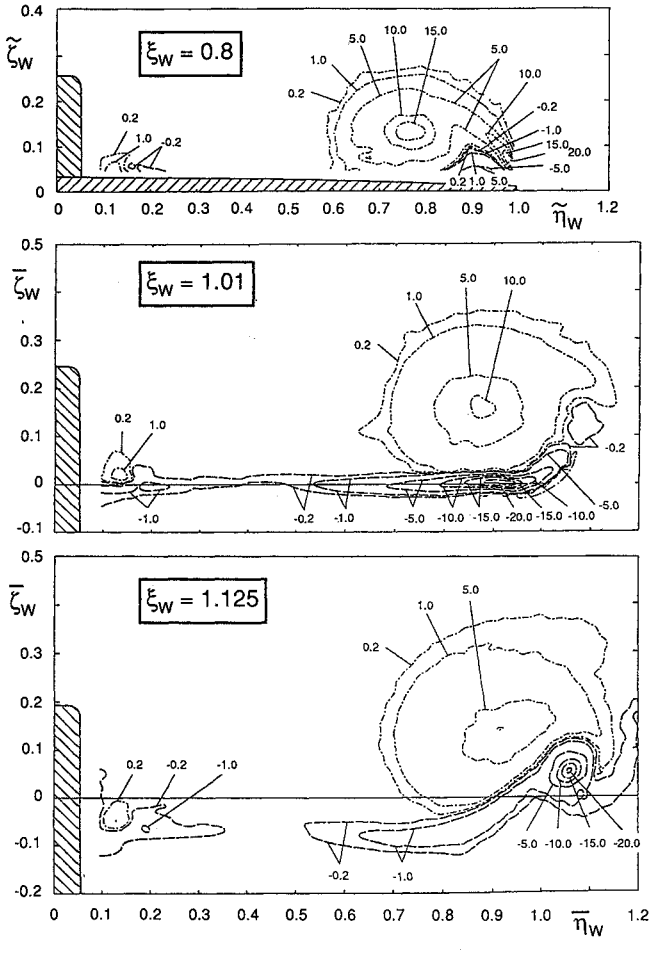

Fig. 9 Results of flowfield measurements over the canard-off configuration at α = 14.6 deg and Re = 1.40 × 10⁶. Lines of constant axial vorticity $\Omega_{\tilde{x}} = \omega_{\tilde{x}} \times s_W/V_\infty$ = const at ξ_W = 0.8, 1.01, and 1.125.

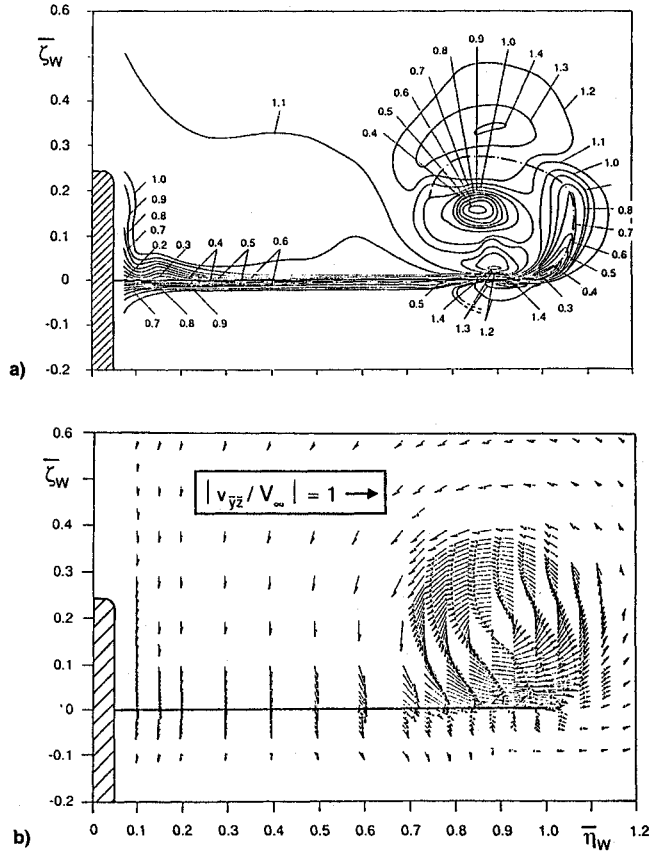

Fig. 10 Results of flowfield measurements at the trailing-edge ξ_W = 1.01 of the canard-off configuration at α = 14.6 deg and Re = 1.40 × 10⁶: a) lines of constant dynamic pressure $c_q = q/q_\infty$ = const and b) velocity vector component $v_{\bar{y}\bar{z}}/V_\infty$ in the measuring plane.

according to Fig. 5 shows that the relative size of the wing vortex system is considerably smaller in this region, and that the flow over the canard-on configuration is distinctly nonconical.

The measuring plane at ξ_W = 0.8 is located slightly upstream of the kink between leading edge and side edge of the wing. The canard's primary vortex has moved further inboard to $\bar{\eta}_W$ = 0.40, $\bar{\zeta}_W$ = 0.25 and the separation of the canard's trailing vortex sheet from the wing surface takes place at $\bar{\eta}_W$ = 0.48. The remains of the canard's trailing-edge vortex can still be identified from the total pressure contours at $\bar{\eta}_W$ = 0.28, $\bar{\zeta}_W$ = 0.34, whereas the lines of constant axial vorticity become circular with respect to the vortex axis. The wing's primary vortex is located at $\bar{\eta}_W$ = 0.8, $\bar{\zeta}_W$ = 0.08 and a secondary vortex detected from axial vorticity of opposite sign is present at about $\bar{\eta}_W$ = 0.87. In the vortex sheet between the leading edge and the primary vortex an area of high axial vorticity in the sense of rotation of the primary vortex is found, and the shape of the vortex sheet shows an irregularity there. This flow pattern has not been found for the canard-off configuration (Figs. 6 and 7), and it can be interpreted as an upstream effect of the vortex formation at the side-edge that will be discussed subsequently.

At the trailing edge of the wing, ξ_W = 1.01, the mixed layer ends at $\bar{\eta}_W$ = 0.50 and the canard's primary vortex is located at $\bar{\eta}_W$ = 0.37, $\bar{\zeta}_W$ = 0.24. Again, the remains of the canard's trailing-edge vortex can be identified from the total pressure contours at $\bar{\eta}_W$ = 0.25, $\bar{\zeta}_W$ = 0.20, but not from the distribution of axial vorticity. The center of the primary vortex of the wing at $\bar{\eta}_W$ = 0.91, $\bar{\zeta}_W$ = 0.10 is surrounded by a vortex sheet of "rectangular" shape. As in the canard-off configuration within the vortex sheet, the shed vorticity drops at some point between the leading edge and the primary vortex, and in the vicinity of this point relatively large total pressure losses as well as increased axial vorticity have been measured. This means that in the canard-on configuration the deformation of the vortex sheet is more pronounced than in the canard-off configuration, and a small double-branched vortex is formed in the vortex sheet at $\bar{\eta}_W$ = 0.99, $\bar{\zeta}_W$ = 0.16, which rotates in the sense of the primary vortex of the wing. This vortex may be called the side-edge vortex. It starts from the region in the vicinity of the kink between leading edge and side edge of the wing, and due to a certain upstream influence its presence is already indicated in the plane at ξ_W = 0.8, as discussed earlier.

The last measuring plane is located at ξ_W = 1.125 downstream of the wing's trailing edge. The canard vortex system including the remains of the canard's trailing-edge vortex at $\bar{\eta}_W$ = 0.29, $\bar{\zeta}_W$ = 0.14 are still easily identified, and the corresponding primary vortex is located at $\bar{\eta}_W$ = 0.37, $\bar{\zeta}_W$ = 0.18. In the region at $\bar{\eta}_W \approx$ 0.55, where the canard's trailing vortex sheet separates from the wing's trailing vortex sheet, areas with increased total pressure losses and enlarged negative axial vorticity are found. This indicates that a small counter-rotating vortex is present there. Its structure is very complicated since it should be "triple-branched," but these details could not be detected with the present probe measuring technique. The wing's primary vortex is located at $\bar{\eta}_W$ = 0.94, $\bar{\zeta}_W$ = 0.09. The wing's trailing vortex sheet rolls up into a counter-rotating trailing-edge vortex that is situated at $\bar{\eta}_W$ = 1.04, $\bar{\zeta}_W$ = 0.05. Remains of the side-edge vortex could not be detected in this measuring plane downstream of the wing.

The documentation of the flow status on this coplanar wing-canard configuration at a low angle of attack and in incompressible flow according to Figs. 11 and 12 is summarized in

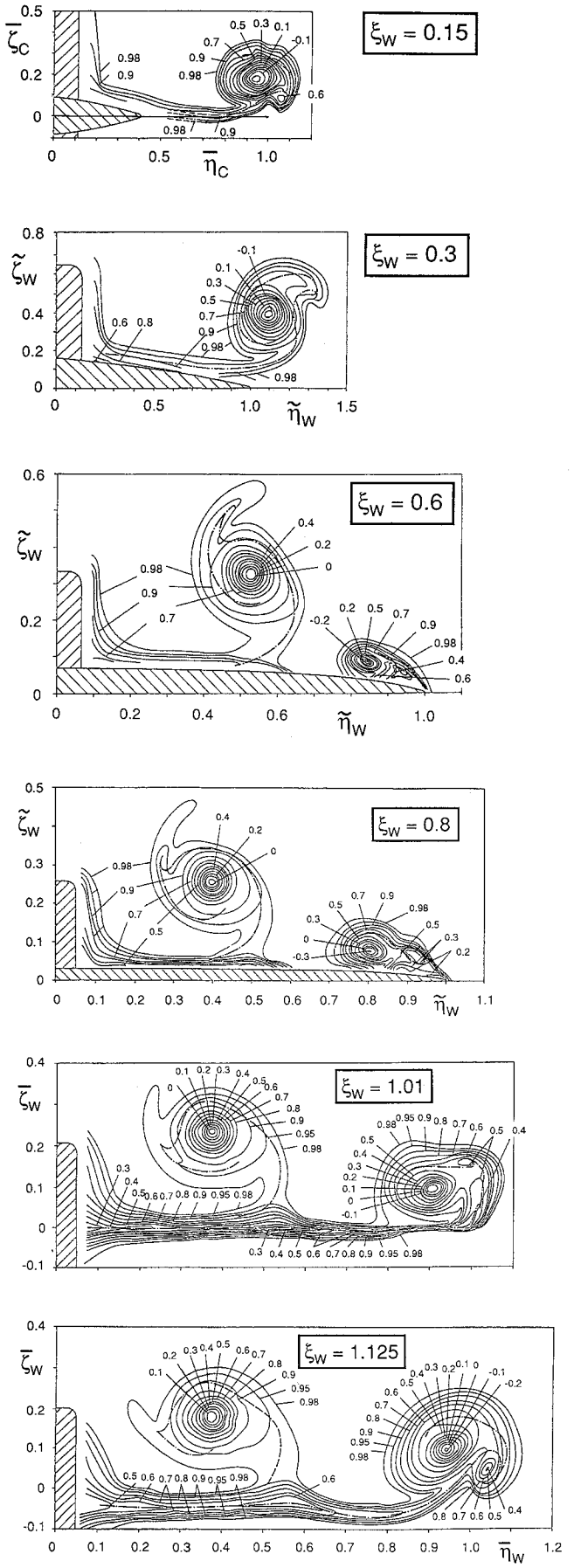

Fig. 11 Results of flowfield measurements over the canard-on configuration at $\alpha = 9.8$ deg and $Re = 1.40 \times 10^6$. Total pressure isobars $c_{pt} = (p_t - p_\infty)/q_\infty$ = const at $\xi_W = 0.15$, 0.30, 0.60, 0.80, 1.01, and 1.125.

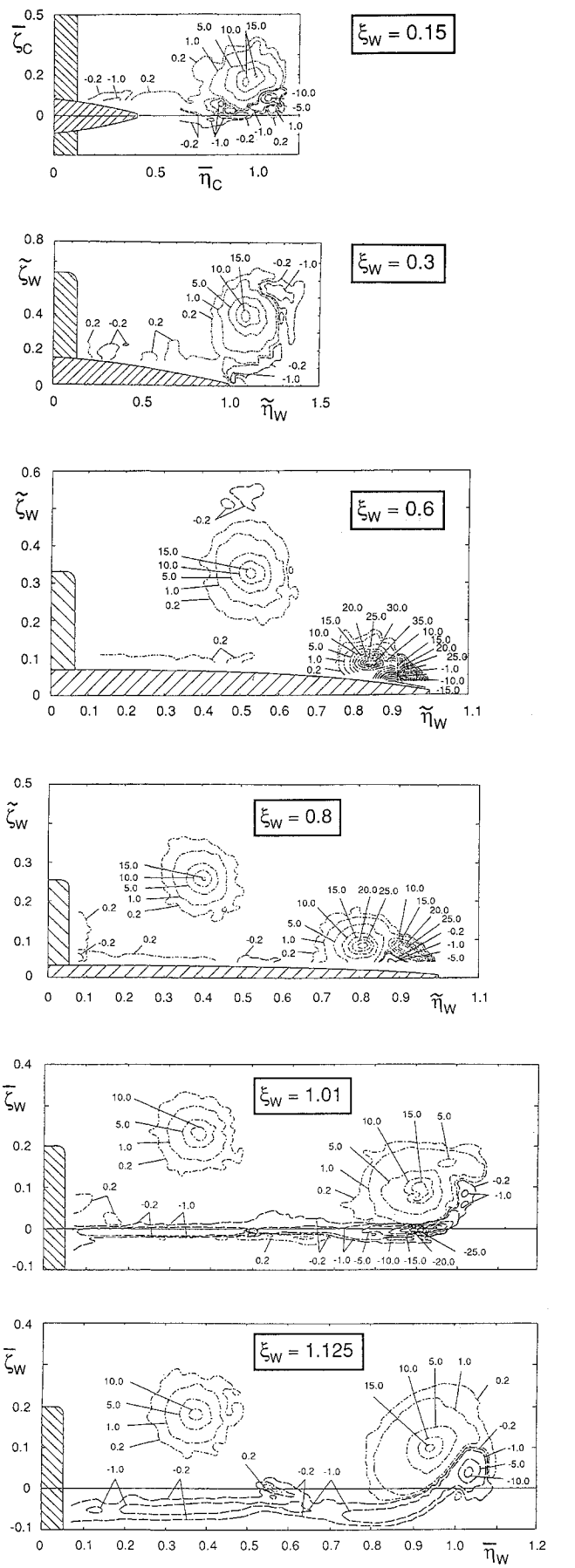

Fig. 12 Results of flowfield measurements over the canard-on configuration at $\alpha = 9.8$ deg and $Re = 1.40 \times 10^6$. Lines of constant axial vorticity $\Omega_{\tilde{x}} = \omega_{\tilde{x}} \times s_W/V_\infty$ = const at $\xi_W = 0.15$, 0.30, 0.60, 0.80, 1.01, and 1.125.

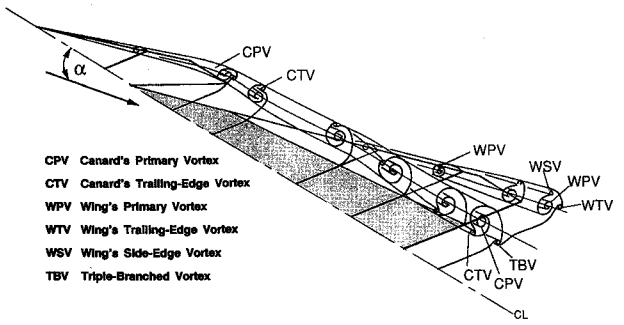

Fig. 13 Schematic view of the flowfield above the canard-on VFE configuration at low angle of attack (inviscid flow).

Fig. 13. For this presentation the effects of viscosity are neglected. This means that secondary separations are not shown. Wing and canard are considered to be flat plates and a fuselage is not taken into account. Figure 13 illustrates how the canard vortex system develops and how this system is located above the wing. In the region of the wing, which is shaded darker than the rest of the wing, the vorticity sheet of the canard merges with the upper surface boundary layer of the wing. This means for the simplified case of Fig. 13 that the free vortex sheet coming from the canard joins the wing-fixed vortex sheet. Therefore, in this region of the wing one combined vortex sheet is present. Figure 13 also illustrates the delayed formation of the wing vortex system in which a side-edge vortex and a trailing-edge vortex are present. Finally, behind the wing one can clearly see a system of at least five vortices on each half of the configuration. These vortices were generated during the course of the flow. There is one primary vortex (CPV, WPV) each for canard and wing that are accompanied by corresponding trailing-edge vortices (CTV, WTV) after having left either the canard's or the wing's trailing edge. In addition, the wing's primary vortex is accompanied by a side-edge vortex (WSV), which is due to the wing planform shape in the tip region. A corresponding side-edge vortex could be (but has not been) detected in the canard's vortex system too. Presumably, a sixth vortex (TBV) on each side of the configuration is associated with the junction of the canard's and the wing's trailing vortex sheets downstream of the wing. Figure 13 demonstrates the complexity of the flow. All these vortices are existing already in inviscid flow. Therefore, if these experimental data are used for comparisons with results of numerical simulations, all these vortices should be included in a proper solution of the Euler equations. In the case of a numerical solution of the Navier-Stokes equations, additional information about the structure of boundary layers, secondary separation regions, and vortex sheets should turn out and these details can again be compared with the present experimental data.

IV. Conclusions

Comprehensive, low-speed aerodynamic investigations have been carried out on a coplanar wing-canard configuration associated with the VFE. Results of three-component balance, surface-pressure, and flowfield measurements are presented for the canard-off and the canard-on configuration. The flowfield measurements were carried out at $\alpha = 9.8$ and 14.6 deg, where vortex breakdown is not present over the configuration.

The main results of these investigations are as follows:

1) On the canard-off configuration a fairly conical vortex formation takes place up to $\xi_W = 0.8$. At the side edge of the wing considerably reduced vorticity is shed that leads to a characteristic deformation of the free vortex sheet in this region. The wing vortex system is accompanied by a counter-rotating trailing-edge vortex.

2) On the canard-on configuration the vortex systems of canard and wing influence each other, but at $\alpha = 9.8$ deg they remain separate from each other up to the region downstream of the trailing edge of the wing. Both vortex systems consist of a primary vortex on each side of the configuration that is accompanied by a trailing-edge vortex. A side-edge vortex has been found in the wing vortex system only.

3) The canard's vortex system passes the wing leading edge relatively high above the configuration. Through wing influence this system moves inward towards the center of the configuration, and also downward towards the wing surface. The canard's trailing vortex sheet merges with the suction-side boundary layer in the inner portion of the wing surface. In nonviscous flow this process is equivalent to a fusion of the canard's free vortex sheet with the bound vortex sheet of the wing. Beneath the canard vortex the canard's vortex sheet separates from the wing surface again and rolls into the canard's vortex system.

4) The canard's downwash leads to a reduction of the wing's effective angle of attack in the front and inner part of the wing. This causes a suppression of flow separation there, and the formation of the wing's leading-edge vortex is therefore delayed. In the outer portions of the wing the canard's upwash supports flow separation, and in addition a side-edge vortex is formed. The wing's primary vortex is fed with vorticity in a different manner than in the canard-off configuration. The wing's vortex system is highly nonconical.

Acknowledgment

These investigations have been supported by Deutsche Forschungsgemeinschaft under Contract DFG-HU 254/8.

References

[1]Behrbohm, H., "Basic Low Speed Aerodynamics of the Short-Coupled Canard Configuration of Small Aspect Ratio," SAAB TN 60, July 1965.

[2]Oelker, H.-Chr., "Aerodynamische Untersuchungen an kurzgekoppelten Entenkonfigurationen bei symmetrischer Anströmung," Dissertation TU Braunschweig 1990, Zentrum für Luft- und Raumfahrttechnik der TU Braunschweig, Forschungsbericht 90-01, Germany, 1990.

[3]Gloss, B. B., and Miner, D. D., "Flow Visualization Study of Close-Coupled Canard-Wing and Strake-Wing Configurations," NASA TM X-75663, 1975.

[4]Er-El, J., and Seginer, A., "Vortex Trajectories and Breakdown on Wing-Canard Configurations," *Journal of Aircraft*, Vol. 22, No. 8, 1985, pp. 641–648.

[5]Er-El, J., "Effect of Wing/Canard Interference on the Loading of a Delta Wing," *Journal of Aircraft*, Vol. 25, No. 1, 1988, pp. 18–24.

[6]Griffin, K. E., "Measurement of Wake Interactions of a Canard and a Forward Swept Wing," U.S. Air Force Academy, USAFA-TN-82-4, Colorado Springs, CO, 1982.

[7]Griffin, K. E., Haerter, E. C., and Smith, B. R., "Wake Characteristics and Interactions of the Canard/Wing Lifting Surface Configuration of the X-29 Forward Swept Wing Flight Demonstrator," U.S. Air Force Academy, USAFA-TN-83-7, Colorado Springs, CO, 1983.

[8]Griffin, K. E., and Jonas, F. M., "Wake Characteristics and Interactions of the Canard Wing Lifting Surface Configuration of the X-29 Forward Swept Wing Flight Demonstrator," AIAA Paper 83-1835, 1983.

[9]Hummel, D., and Oelker, H.-Chr., "Vortex Interference Effects on Close-Coupled Canard Configurations in Incompressible Flow," *Proceedings Symposium "International Vortex Flow Experiment on Euler Code Validation"* (Stockholm, Sweden), FFA, Flygtekniska Forsöksanstalten, Bromma, Sweden, 1986, pp. 47–61.

[10]Oelker, H. Chr., and Hummel, D., "Experimentelle Untersuchungen an Entenkonfigurationen," DGLR-Bericht 86-03, 1986, pp. 172–191.

[11]Oelker, H. Chr., and Hummel, D., "Investigations on the Vorticity Sheets of a Close-Coupled Delta-Canard Configuration," *ICAS-Proceedings 1988*, Vol. 1, 1988, pp. 649–662; see also *Journal of Aircraft*, Vol. 26, No. 7, 1989, pp. 657–666.

[12]Hummel, D., and Oelker, H. Chr., "Effects of Canard Position on the Aerodynamic Characteristics of a Close-Coupled Canard Configuration at Low Speed," AGARD-CP-465, 1989, pp. 7-1–7-18; see

also *Zeitschrift für Flugwissenschaften und Weltraumforschung*, Vol. 15, No. 2, 1991, pp. 74–88.

[13]Drougge, G., "The International Vortex Flow Experiment for Computer Code Validation," *ICAS-Proceedings 1988*, Vol. 1, 1988, pp. XXXV–XLI.

[14]Elsenaar, A., Hjelmberg, L., Bütefisch, K., and Bannink, W. J., "The International Vortex Flow Experiment," AGARD-CP-437, 1988, pp. 9-1–9-23.

[15]Williams, B. R., Kordulla, W., Borsi, M., and Hoeijmakers, H. W. M., "Comparison of Solution of Various Euler Solvers and One Navier-Stokes Solver for the Flow About a Sharp-Edged Cropped Delta Wing," AGARD-CP-494, 1991, pp. 2-1–2-12.

[16]Van den Berg, J. I., Hoeijmakers, H. W. M., and Jacobs, J. M. J. W., "Analysis of an Euler-Equation Method Applied to Leading-Edge Vortex Flow," AGARD-CP-494, 1991, pp. 4-1–4-12.

[17]Borsi, M., Formaggia, L., Hettena, E., Santillan, S., Selmin, V., and Tarditi, S., "Vortical Flow Simulation by Using Structured and Unstructured Grids," AGARD-CP-494, 1991, pp. 3-1–3-12.

[18]Longo, J. M. A., and Das, A., "Numerical Simulation of Vortical Flows over Close-Coupled Canard-Wing Configuration," AIAA Paper 90-3003, Aug. 1990.

[19]Hilgenstock, A., and Vollmers, H., "On the Simulation of Compressible Turbulent Flows Past Delta Wing, Delta Wing-Body and Delta Wing-Canard," AGARD-CP-494, 1991, pp. 7-1–7-13.

[20]Tu, E. L., "Navier-Stokes Simulation of a Close-Coupled Canard-Wing-Body Configuration," AIAA Paper 91-0070, Jan. 1991.

[21]Hummel, D., "On the Vortex Formation over a Slender Wing at Large Angles of Incidence," AGARD-CP-247, 1978, pp. 15-1–15-17.